Applied Mathematical Modelling 39 (2015) 820–837

Contents lists available at ScienceDirect

Applied Mathematical Modelling

journal homepage: www.elsevier.com/locate/apm

Hysteresis and temperature-induced transitions in ferromagnetic materials

Alessia Berti [a,*], Claudio Giorgi [b], Elena Vuk [b]

[a] Università Telematica e-Campus, Facoltà di Ingegneria, Via Isimbardi 10, 22060 Novedrate, CO, Italy
[b] Università di Brescia, DICATAM, via Valotti 9, 25133 Brescia, Italy

ARTICLE INFO

Article history:
Received 8 March 2013
Received in revised form 13 April 2014
Accepted 8 July 2014
Available online 21 July 2014

Keywords:
Phase transformations in solids
Ferromagnetic–paramagnetic transition
Ginzburg–Landau equation
Problems involving hysteresis
Magnetic susceptibility
Curie–Weiss law

ABSTRACT

In this paper we present two basic one-dimensional models for the temperature-induced phase-changes in a ferromagnetic material. In the framework of the Ginzburg–Landau theory, we construct suitable thermodynamic potentials from which thermodynamically-consistent evolution equations for the magnetization are derived. For both *soft* and *hard* materials these models account for saturation and provide an effective description of the transition from paramagnetic to ferromagnetic regimes by displaying the onset of hysteresis loops when the temperature decreases below the Curie critical value. The temperature enters the model as a parameter by way of the magnetic susceptibility. Such a dependence is discussed in order to comply with both Bloch's law (below the critical value) and Curie–Weiss law (far above the critical value). Focusing on uniform processes, numerical simulations of the magnetic responses at different temperatures are performed.

1. Introduction

In metals like iron, cobalt, nickel and many alloys containing these elements, a small external magnetic field yields a large magnetization inside the material, due to the alignment of the spin magnetic moments. This typical phenomenon is called *ferromagnetism*. Atomic moments in ferromagnetic materials exhibit very strong interactions (due to exchange forces) that result in their parallel alignment. Below the critical value θ_c, called *Curie temperature*, this parallel alignment produces a large net magnetization, even if the applied external field is removed, so giving rise to a spontaneous magnetization [1,2]. On the contrary, when the temperature overcomes the critical value θ_c, the residual alignment disappears and the material reverts to the paramagnetic behavior. The passage from the paramagnetic to the ferromagnetic behavior and vice versa is usually evaluated as a second-order phase transition (see, for instance, [3,4]): no latent heat is released or absorbed during the phase change at zero external field, as in superconductivity. Unlike that, however, the ferromagnetic transition involves hysteresis. Artfully, we succeed here in emphasizing their differences and similarities by comparing the diagram in Fig. 6 with the usual representation (Fig. 7) of the critical magnetic field versus temperature in superconductivity [5].

Many mathematical models have been proposed to describe the occurrence of hysteresis loops in real-world materials. A large part of them are devoted to the accurate modeling of ferromagnetic hysteresis and are widely used in the industry. In particular, we mention the physics-based Jiles–Atherton model and a lot of phenomenological models of Duhem and Preisach type (see, for instance, [6,3,7] for more details). However, these models lose the connection with thermodynamics and

* Corresponding author.
E-mail addresses: alessia.berti@unibs.it (A. Berti), claudio.giorgi@unibs.it (C. Giorgi), elena.vuk@unibs.it (E. Vuk).

http://dx.doi.org/10.1016/j.apm.2014.07.004
0307-904X/

the energy consistency is not ensured. Although very effective in a great variety of isothermal applications, they are unable to account for the ferromagnetic temperature-induced transition.

In order to model how temperature variations induce phase changes involving hysteresis, a different approach is needed. Among all those which rely on a consistent thermodynamic formulation, the simplest strategy consists in applying the phase-field machinery and the Ginzburg–Landau theory [3,8]. A first attempt to model the ferromagnetic transition in this framework traces back to Ginzburg [9]. Recently, further efforts have been spent in this direction and some improvements have been obtained [10–13].

The main advantage to apply the Ginzburg–Landau machinery to transition phenomena with hysteresis consists in its simplicity. The modeling procedure starts from identifying the proper scalar- or vector-valued order parameter (the so called *phase-field*). Then, the exploitation of thermodynamic restrictions leads to the consistent form of the phase variable evolution, which is governed by a single function, the Gibbs free energy [14]. In scalar models, after selecting (or constructing) the suitable Gibbs free energy density ψ of the system, the evolution of the phase-field φ is ruled by the so-called *Ginzburg–Landau equation*

$$\rho\dot{\varphi} = -\kappa((\rho\partial_{\varphi}\hat{\psi}) - \nabla\cdot(\rho\partial_{\nabla\varphi}\hat{\psi})), \tag{1}$$

where ρ is the mass density, κ a positive constant and $\hat{\psi} = \psi/\theta$.

For the ferromagnetic case, we refer to [12], where a thermodynamically consistent derivation of a general vector-valued phase-field equation of the Ginzburg–Landau type is devised. Unlike other kinds of magnetic hysteresis models (as Duhem and Preisach, for instance), this phase-field evolution equation is naturally energy consistent. In addition, if coupled with customary balance equations (mass, momentum, internal energy and, possibly, Maxwell equations), it gives rise to a system which is quite easy to handle even in the three dimensional case (see, for instance, [11]). On the other hand, we mention that not all typical features of hysteresis can be represented by means of phase-field models. For instance, they are unable to account for minor hysteresis loops [15]. In addition, they establish a relation between the magnetization and the applied external magnetic field that does not fulfill the rate-independence property.

The Ginzburg–Landau machinery is widely used in modeling hysteretic first-order transitions (in shape memory alloys, for instance, see [16,8]), but few papers apply it when ferromagnetic hysteresis is involved (e.g. [3,11,13]). All of them give a naive description of the onset of the hysteretic regime and no evidence of the effectiveness of this modeling approach. Just in [13] some numerical simulations are performed. In our opinion, there are two difficulties that reduce the development of this approach in modeling hysteretic phenomena. The former is a problem due to thermodynamic principles: in materials with memory the free enthalpy is not unique (up to a constant), but there are infinitely many (sub) potentials (really, a convex set) which obey the Second Law [17]. The latter consists in a mathematical problem: if thermodynamic potentials are replaced by their polynomial expansion in the phase variable, as usual, it is impossible to account for saturation (that is, confinement of the phase variable in $[0,1]$). In a different background, this obstacle may be overcome by proving a "maximum principle theorem" for the phase variable. Unfortunately, in the ferromagnetic context this strategy is out of reach.

The aim of this paper is to develop the approach carried out in [12] by improving previous models devised in [3,11,13]. The first novelty is physics-based: starting from the proper distinction between external and internal magnetic field, we take advantage of introducing the Weiss molecular mean field. Then, we construct the explicit expression of the Gibbs free energy potential on the basis of the shape of the "skeleton" curve. Two kinds of these curves are considered in the sequel and referred to as "bilinear" and "Langevin". Accordingly, two new families of (non polynomial) energy potentials are generated and inserted into the evolution Eq. (1), so yielding two simple Ginzburg–Landau-like models which account for saturation. From a theoretical point of view, the stability of each phase is scrutinized by way of the temperature-dependent non-convexity of these potentials. In order to achieve some evidence of the effectiveness of our modeling approach in capturing the phase-change dynamics for practical purposes, some numerical simulations of the hysteresis loops are performed in both "bilinear" and "Langevin" cases under cyclic conditions.

1.1. Plan of the paper

The plan of the paper is the following. The sequel of this section is devoted to introduce Maxwell's equations inside the matter and distinguish the internal magnetic field, H, from the external (applied) one, H_{ex}. In Section 2, we state the relation between H and the magnetization M governing a paramagnetic material. Then, some trial one-dimensional models are exhibited and their "skeleton curve" are pointed out. Taking advantage of the Weiss theory, in Section 3 we discuss the mathematical modeling of a ferromagnetic material with a view to describe the temperature-induced transition process. Such a representation is based on the temperature-dependent shape of the "skeleton curve" which allows us, in Section 4, to construct the Gibbs potential and then to apply the Ginzburg–Landau theory. In order to check the resulting model, we present some numerical simulations that clarify the ease of applying this approach. Section 5 is devoted to represent hysteresis in the (H_{ex}, M)-plane. Therein, we show that different shapes of the hysteresis major loop (for instance, in soft and hard ferromagnetic substances) can be originated by the same Ginzburg–Landau model for different values of constitutive parameters. At the end of this section we exhibit some numerical simulations. Finally, applying the Curie–Weiss and Bloch's law, in Section 6 we establish the general form (with respect to temperature) of the ferromagnetic susceptibility involved in our bilinear model of soft materials.

1.2. Constitutive and Maxwell's equations inside the matter

Let us consider a rigid magnetic conductor at rest which occupies a domain $\Omega \subset \mathbb{R}^3$. For simplicity, we suppose that its mass density is constant. Inside the body, we denote by $\boldsymbol{E}$, $\boldsymbol{H}$, $\boldsymbol{D}$, $\boldsymbol{B}$ the electric field, the magnetic field, the electric displacement and the magnetic induction. At any point $x \in \Omega$ the behavior of the material is ruled by Maxwell's equations

$$\nabla \times \boldsymbol{E} = -\dot{\boldsymbol{B}}, \quad \nabla \cdot \boldsymbol{B} = 0,$$
$$\nabla \times \boldsymbol{H} = \dot{\boldsymbol{D}} + \boldsymbol{J}, \quad \nabla \cdot \boldsymbol{D} = \rho_e,$$

where $\boldsymbol{J}$ is the current density and ρ_e is the free charge density. Since inside a magnetic material the displacement current $\dot{\boldsymbol{D}}$ is negligible if compared with $\boldsymbol{J}$, throughout the paper we assume for simplicity

$$\dot{\boldsymbol{D}} = \boldsymbol{0}, \quad \rho_{\mathbf{e}} = \boldsymbol{0}, \quad \boldsymbol{J} = \sigma \boldsymbol{E},$$

where σ is the electric conductivity. These choices lead to

$$\nabla \times \boldsymbol{E} + \dot{\boldsymbol{B}} = 0, \quad \nabla \cdot \boldsymbol{B} = 0, \tag{2}$$

$$\nabla \times \boldsymbol{H} - \sigma \boldsymbol{E} = 0. \tag{3}$$

In free space the magnetic induction $\boldsymbol{B}$ is proportional to the *applied external magnetic field* $\boldsymbol{H}_{\text{ex}}$, namely $\boldsymbol{B} = \mu_0 \boldsymbol{H}_{\text{ex}}$, where μ_0 denotes the permeability constant of free space. On the other hand, inside the matter $\boldsymbol{B}$ admits the classical decomposition:

$$\boldsymbol{B} = \mu_0(\boldsymbol{H} + \boldsymbol{M}), \tag{4}$$

where $\boldsymbol{H}$ is the *internal magnetic field* and $\boldsymbol{M}$ is the *matter magnetization*. The field $\boldsymbol{H}$ consists of the applied external field $\boldsymbol{H}_{\text{ex}}(x)$ acting in a point x, plus any self-field due to the surrounding matter (see, for instance, [1, Ch. 2]). Accordingly, inside the matter we should define the *internal magnetic field* $\boldsymbol{H}$ as follows

$$\boldsymbol{H} = \boldsymbol{H}_{\text{ex}} - \mathbb{A}\boldsymbol{M}, \tag{5}$$

where $\mathbb{A}$ is a positive-definite tensor depending on the shape and anisotropy of the material. According to the Brown approximation, $\mathbb{A}$ can be split into the sum of a *demagnetizing* and a *purely anisotropic tensor* (see [18, p. 48]).

Remark 1. If $\boldsymbol{n}$ represents some eigenvector of $\mathbb{A}$, then along this direction (5) becomes

$$H = H_{\text{ex}} - \alpha M, \tag{6}$$

where $\alpha > 0$ is the eigenvalue related to $\boldsymbol{n}$ and

$$H = H \cdot \boldsymbol{n}, \quad H_{\text{ex}} = \boldsymbol{H}_{\text{ex}} \cdot \boldsymbol{n}, \quad M = \boldsymbol{M} \cdot \boldsymbol{n}.$$

In order to prove these relations, we represent $\boldsymbol{M} = M\boldsymbol{n} + M^{\perp}\boldsymbol{m}$, where $\boldsymbol{m} \cdot \boldsymbol{n} = 0$ and $|\boldsymbol{m}| = 1$, and then we have

$$\mathbb{A}\boldsymbol{M} \cdot \boldsymbol{n} = M\mathbb{A}\boldsymbol{n} \cdot \boldsymbol{n} + M^{\perp}\mathbb{A}\boldsymbol{m} \cdot \boldsymbol{n}.$$

By assumption $\mathbb{A}\boldsymbol{n} \cdot \boldsymbol{n} = \alpha$ and then

$$\mathbb{A}\boldsymbol{m} \cdot \boldsymbol{n} = \mathbb{A}\boldsymbol{n} \cdot \boldsymbol{m} = \alpha \boldsymbol{n} \cdot \boldsymbol{m} = 0.$$

Accordingly, $\mathbb{A}\boldsymbol{M} \cdot \boldsymbol{n} = \alpha M$ and (6) follows (cf. Eq. (6.14) in [12]).

A lot of magnetic materials exhibits a non-linear anisotropic relation between $\boldsymbol{H}$ and $\boldsymbol{M}$. From the mathematical point of view, anisotropy entails that the direction of $\boldsymbol{M}$ does not coincide with the direction of the internal field $\boldsymbol{H}$. The most common anisotropy effect is connected to the existence of one easy direction, and in literature this is referred to as *uniaxial anisotropy*.

2. Paramagnetic materials

In a paramagnetic material occupying a three-dimensional domain Ω, the values of $\boldsymbol{H}(x)$ and $\boldsymbol{M}(x)$ in a point $x \in \Omega$ are related by a homogeneous, nonlinear and (possibly) non-isotropic function $\boldsymbol{f}$ which depends also on the absolute temperature at the same point, $\theta(x)$. Thus,

$$\boldsymbol{M}(x) = \boldsymbol{f}(\boldsymbol{H}(x), \theta(x)), \quad \boldsymbol{f}(\boldsymbol{0}, \cdot) = \boldsymbol{0}. \tag{7}$$

Henceforth, we confine our analysis to the one-dimensional case by choosing $\boldsymbol{n}$ as in (6). Remark 1 allows us to simply represent (7) in the scalar form

$$M = f(H, \theta), \quad f(H, \theta) = \boldsymbol{f}(H\boldsymbol{n}, \theta) \cdot \boldsymbol{n}. \tag{8}$$

As customary, we assume

(F.1) f is monotone increasing w.r.t. H and $f(0,\cdot)=0$,
(F.2) $\lim_{H\to\pm\infty} f(H,\cdot)=\pm M_s$,

where $M_s>0$ represents the *saturation magnetization* in the $\boldsymbol{n}$-direction. As a consequence, the *internal magnetic susceptibility* (in the $\boldsymbol{n}$-direction), which is defined as the partial derivative of f w.r.t. H, namely

$$\chi(H,\theta)=\partial_H f(H,\theta) \tag{9}$$

is positive and fulfills the asymptotic condition

$$\lim_{|H|\to\infty}\chi(H,\cdot)=0.$$

By virtue of (6)–(8) and $F.1$–$F.2$, we can infer the constitutive relation between M and H_{ex}. Actually, letting $f_\theta(H)=f(H,\theta)$ we have $f_\theta^{-1}(M)=H_{\text{ex}}-\alpha M$, and this yields

$$H_{\text{ex}}=f_\theta^{-1}(M)+\alpha M,$$

where the r.h.s. is a monotone increasing function of M, as well as f_θ^{-1}. Then, we obtain

$$M=\tilde{f}(H_{\text{ex}},\theta)\quad \tilde{f}=(f_\theta^{-1}+\alpha I)^{-1}. \tag{10}$$

According to this approach, we define the *external magnetic susceptibility* as

$$\chi_{\text{ex}}(H_{\text{ex}},\theta)=\partial_{H_{\text{ex}}}\tilde{f}(H_{\text{ex}},\theta).$$

It is related to the internal susceptibility χ by the following relations

$$\chi_{\text{ex}}(H_{\text{ex}},\cdot)=\frac{\chi(H,\cdot)}{1+\alpha\chi(H,\cdot)},\quad \chi(H,\cdot)=\frac{\chi_{\text{ex}}(H_{\text{ex}},\cdot)}{1-\alpha\chi_{\text{ex}}(H_{\text{ex}},\cdot)}. \tag{11}$$

In particular, letting $\chi_0(\theta)=\chi(0,\theta)$,

$$\chi_{\text{ex}}(0,\theta)=\frac{\chi_0(\theta)}{1+\alpha\chi_0(\theta)}>0.$$

In addition, $(F.1)$ and $(F.2)$ are satisfied even by $\tilde{f}$.

2.1. Some basic models

First, we choose f in (8) as a simple bilinear function

$$f_b(H,\theta)=\begin{cases}\chi_0(\theta)H & \text{if } |H|<H^*,\\ M_s & \text{if } H\geqslant H^*,\\ -M_s & \text{if } H\leqslant -H^*,\end{cases} \tag{12}$$

where $H^*(\theta)=M_s/\chi_0(\theta)$. This function is monotone non-decreasing and strictly increasing in $(-H^*,H^*)$. A more realistic (and physically sound) form of f is due to Langevin,

$$f_L(H,\theta)=M_s[\coth(H/H_*(\theta))-H_*(\theta)/H], \tag{13}$$

where $H_*=H^*/3$. The graphs of f_b and f_L in the (H,M)-plane are depicted in Fig. 1.

According to these choices of f, the magnetic susceptibility (9) takes respectively the following forms,

$$\chi_b(H,\theta)=\begin{cases}\chi_0(\theta) & \text{if } |H|<H^*,\\ 0 & \text{otherwise},\end{cases}$$

$$\chi_L(H,\theta)=\frac{M_s}{H_*(\theta)}\left[1-\coth^2(H/H_*(\theta))+(H_*(\theta)/H)^2\right].$$

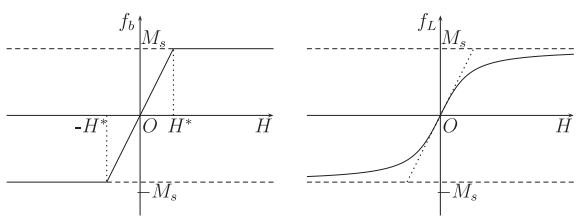

Fig. 1. The graphs of f_b and f_L ($M_s=\chi_0=2$).

Because of the assumed relation $H^* = 3H_*$, we have

$$\lim_{H\to 0}\chi_L(H,\theta) = \frac{M_s}{3H_*(\theta)} = \chi_0(\theta).$$

Both these approaches hold true in a thermodynamic framework, in that the shape of f modifies when the value of the temperature changes. In particular, we expect the Curie's law is recovered in the limit of high temperatures. To this end, let H_* linearly depend on the temperature,

$$H_*(\theta) = \ell\theta, \quad \ell = Nk_B/M_s,$$

where N is the number of atoms per unit volume and k_B represents the Boltzmann constant (see, for instance, [2, Section 1.2.]). Then,

$$\chi_0(\theta) = \frac{M_s}{3\ell\theta} = \frac{C}{\theta}, \quad C = \frac{M_s^2}{3Nk_B} \tag{14}$$

and we recover the Curie's law for the Langevin function (13) at $H = 0$,

$$\lim_{H\to 0}\chi_L(H,\theta) = \frac{C}{\theta}.$$

When the bilinear function f_b is involved, by virtue of (14) the Curie's law holds true in the whole interval $(-3\ell\theta, 3\ell\theta)$. The graphs of $\chi_b(\cdot,\theta)$ and $\chi_L(\cdot,\theta)$ at different temperatures, say θ and $\theta/2$, are depicted in Fig. 2.

Remark 2. The Curie's law holds true even in the $H_{\text{ex}} - M$ representation, as usual. Indeed, if $\chi(H,\theta) \approx C/\theta$ holds, then from $(11)_1$ we have

$$\chi_{\text{ex}}(H_{\text{ex}},\theta) = \frac{\chi(H,\theta)}{1+\alpha\chi(H,\theta)} \approx \frac{C}{\theta}$$

provided that $\theta \gg \alpha C$. In particular,

$$\chi_{\text{ex},b}(H_{\text{ex}},\theta) = \begin{cases} C/(\theta+\alpha C) & \text{if } |H_{\text{ex}}| < 3\ell\theta + \alpha M_s, \\ 0 & \text{otherwise.} \end{cases}$$

3. Ferromagnetic transition

Henceforth, we confine our analysis to the one-dimensional case by choosing $\boldsymbol{n}$ as in (6). Unlike paramagnets, ferromagnetic materials exhibit *two distinct regimes* which depend on the temperature. In the paramagnetic regime, which occurs above a characteristic temperature θ_c called the (magnetic) *Curie temperature,* a relation like (8) holds. In the ferromagnetic regime (below θ_c) the relation between H and M is no longer expressed in terms of a single-valued function, and the pair (H, M) moves along a continuous curve which changes according to the increasing or decreasing of H. This provides the standard hysteretic behavior (see, for instance, [18,19,2] and references therein). In particular, for large values of $|H|$, say $|H| > H_c$, the magnetization of the material reaches a saturation value.

With some approximation, possibly, we can identify two regions in the (H, M)-strip: the rectangle containing the major loop, where $|H| \leqslant H_c$, and two unbounded strips, $H > H_c$ and $H < -H_c$, where lie the hysteresis tails (see, for instance, Figs. 3c and 4c). This simplified picture allows us to introduce the notion of two distinct *phases* in ferromagnets.

Definition 1. At a given temperature, the "matched phase" corresponds to a biunivocal relation between H and M, whereas the "unmatched phase" corresponds to a multivalued relation between these fields. When $\theta \geqslant \theta_c$, the paramagnetic regime involves the matched phase, only. As $\theta < \theta_c$, the ferromagnetic regime involves both phases, depending on the values of H: the matched phase when $|H| > H_c$ and the unmatched phase when $|H| \leqslant H_c$.

This suggestion relies on a quite basic physical motivation. In the paramagnetic regime, for any applied field H the magnetic moment arrangements lead to a single value of the resultant moment M. In the ferromagnetic regime, at values of H below some threshold H_c, different values of M are allowed, depending on different size and number of magnetic domains

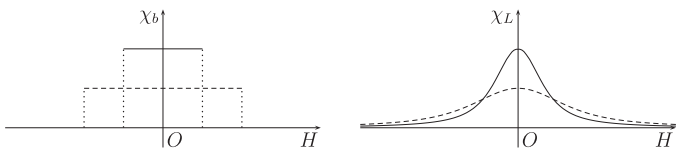

Fig. 2. The graphs of χ_b and χ_L at different temperatures: θ (solid) and $\theta/2$ (dashed).

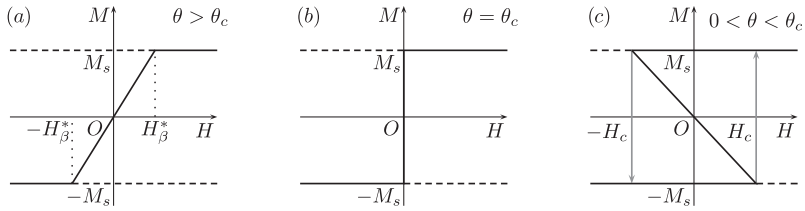

Fig. 3. The graphs of $f_{b,\beta}$ when: (a) $0 < \beta < 1/\chi_0$, (b) $\beta = 1/\chi_0$ and (c) $\beta > 1/\chi_0$.

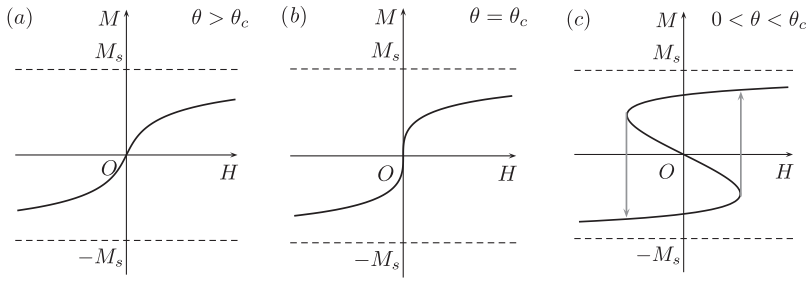

Fig. 4. The graphs of $f_{L,\beta}$ when: (a) $0 < \beta < 1/\chi_0$, (b) $\beta = 1/\chi_0$ and (c) $\beta > 1/\chi_0$.

(the "unmatched phase"). By increasing the value of H, magnetic domains are forced to align with it, but above the threshold value H_c such an increase cannot cause further alignment of the domains and a saturation value of M is reached (the "matched phase").

In addition, this statement enables the distinction between temperature-induced (at fixed H) and magnetic-field-induced (at fixed θ) phase transitions, which can be depicted with the help of a (θ, H)-diagram (see Figs. 5 and 6). As a consequence, a lot of different phase transitions can be compared with it. For instance, we can establish a connection between ferromagnetic and superconductive transitions (see subSection 3.3). By letting the magnetic field M correspond to the stress σ whereas the magnetization M correspond to the elongation ε, we can also establish a comparison between the (θ, H)-diagram in ferromagnets and the (θ, σ)-diagram in shape memory alloys. To our knowledge, all these arguments are new.

In order to mathematically describe this approach, we exploit the Weiss theory which is based on the introduction of the *local magnetic field* H_{loc}. It no longer coincides with the internal field acting inside the material, but it is given by the superposition of H and a (fictitious) *molecular mean field*,

$$H_{\text{w}} = \beta M,$$

where the Weiss's factor β is a positive parameter depending on the molecular fields and related to the Curie temperature θ_c, as it will be specified in (22). Accordingly,

$$H_{\text{loc}} = H + \beta M = H_{\text{ex}} - (\alpha - \beta)M. \tag{15}$$

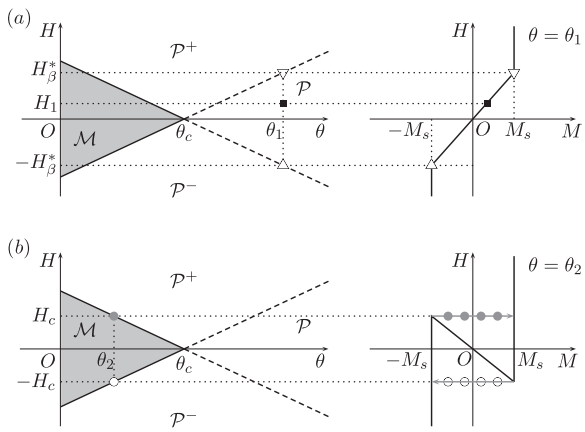

Fig. 5. The (θ, H)-diagram and the graph of $f_{b,\beta}$ when: (a) $\theta = \theta_1 > \theta_c$, (b) $\theta = \theta_2 < \theta_c$.

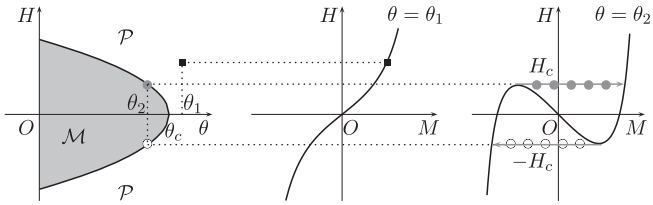

Fig. 6. The (θ, H)-diagram in the Langevin case and the graphs of $f_{L,\beta}$ when $\theta = \theta_1 > \theta_c$ (at the center) and $\theta = \theta_2 < \theta_c$ (on the right).

Here, the parameter β is empirically defined. Its rigorous deduction would take into account ferromagnetic coupling and requires a quantum mechanical calculation (see, for instance, [2]).

The Weiss approach is very useful in attacking many problems of ferromagnetism. Indeed, it allows a mathematical treatment of a ferromagnetic material similar to that used for paramagnetic substances. Actually, this approach prescribes that the value of M in a point $x \in \Omega$ must be regarded as a function of H_{loc}, instead of H, at the same point (see [1] and also [12, Section 8.1]). The Giles-Atherton model, for instance, takes advantage of this [20]. When applied to (8), this procedure leads to

$$M = f(H_{\text{loc}}, \theta) = f_\theta(H_{\text{loc}}), \tag{16}$$

where f is exactly the same function as in (8). Accordingly, we define the *local magnetic susceptibility*

$$\chi(H_{\text{loc}}, \theta) = \partial_{H_{\text{loc}}} f(H_{\text{loc}}, \theta) > 0, \quad \chi(0, \theta) = \chi_0(\theta).$$

As a consequence, from (15) and (16) we have

$$H = g_\beta(M, \theta) = f_\theta^{-1}(M) - \beta M. \tag{17}$$

Since the r.h.s. is an increasing function of M if $\beta = 0$, then g_β remains increasing when $0 < \beta < \beta^*$, for a sufficiently small value of β^* which depends on the shape of f. In this range, g_β can be reverted,

$$M = f_\beta(H, \theta). \tag{18}$$

Because of the positivity of β, when $\beta \geqslant \beta^*$ the monotone character of f could not be conserved by f_β, as it will be discussed henceforth. Nevertheless, for practical purposes, g_β is assumed to be piecewise monotone for all $\beta > 0$, so that it can be (at least piece-wisely) inverted. In both cases, we refer to the graph of f_β as the *skeleton curve* of the model.

3.1. Transition in the bilinear case

In this special case, we apply the relation (16) to the skeleton curve $f = f_b$, namely

$$f_b(H_{\text{loc}}, \theta) = \begin{cases} \chi_0(\theta) H_{\text{loc}} & \text{if } |H_{\text{loc}}| < H^*, \\ M_s & \text{if } H_{\text{loc}} \geqslant H^*, \\ -M_s & \text{if } H_{\text{loc}} \leqslant -H^*. \end{cases} \tag{19}$$

By virtue of (15), relation (18) takes the form

$$M = f_{b,\beta}(H, \theta) = \begin{cases} \chi_\beta(\theta) H & \text{if } |H| < |H^*_\beta(\theta)|, \\ M_s & \text{if } H \geqslant H^*_\beta(\theta), \\ -M_s & \text{if } H \leqslant -H^*_\beta(\theta), \end{cases} \tag{20}$$

where

$$\chi_\beta(\theta) = \frac{\chi_0(\theta)}{1 - \beta\chi_0(\theta)}, \quad H^*_\beta(\theta) = [1 - \beta\chi_0(\theta)]H^* = \frac{M_s}{\chi_\beta(\theta)}. \tag{21}$$

We stress that $\chi_\beta > \chi_0$ if $0 < \beta < 1/\chi_0$, and $f_{b,\beta}$ is a monotone increasing function as well as f_b. Otherwise, $\chi_\beta < 0$ and $f_{b,\beta}$ is no longer a function, but a curve that looks like a reversed zed (see Fig. 3c).

A thermodynamic framework can be achieved by the following

Remark 3. Let θ_c denote the Curie's *transition temperature* and let

$$\beta = \theta_c / C. \tag{22}$$

Then, from (21) we recover the Curie–Weiss law

$$\chi_\beta(\theta) = \frac{C}{\theta - \theta_c},$$

where C is given in (14). This law holds for all temperatures $\theta > \theta_c$ and is restricted to the range

$$-3\ell(\theta - \theta_c) \leqslant H \leqslant 3\ell(\theta - \theta_c).$$

A transition from paramagnetic to ferromagnetic regime occurs when β equals $1/\chi_0$, namely at the temperature $\theta = \theta_c$. The material is in the paramagnetic phase when $\theta > \theta_c$, so that $0 < \beta < 1/\chi_0$ and $\chi_\beta > \chi_0 > 0$ (see Fig. 3a). Otherwise, the ferromagnetic phase occurs when $0 < \theta < \theta_c$, so that $\beta > 1/\chi_0$ and $-1/\beta < \chi_\beta < 0$ (see Fig. 3c). Then, the *internal coercive field* is given by $H_c = -H^*_\beta$.

It is worth noting that χ_β can be identified with the internal ferromagnetic susceptibility only when $\theta > \theta_c$. Otherwise, it merely represents the (negative) slope at $H = 0$ of the skeleton curve. The proper form of the ferromagnetic susceptibility at $\theta < \theta_c$ will be scrutinized in Section 6.

3.2. Transition in the Langevin case

In order to construct a more realistic model, the skeleton curve f may be chosen equal to the Langevin function f_L, namely

$$M = f_L(H_{\text{loc}}, \theta) \equiv M_s[\coth(H_{\text{loc}}/H_*(\theta)) - H_*(\theta)/H_{\text{loc}}].$$

By letting $\mathbb{L}(u) = \coth u - 1/u$, this relation may be rewritten as $M/M_s = \mathbb{L}(H/H_*)$. Then, applying (17) with $f = f_L$, we have

$$H = \mathcal{L}_\beta(M, \theta) \equiv H_*(\theta)\mathbb{L}^{-1}(M/M_s) - \beta M \tag{23}$$

and the skeleton curve $f_{L,\beta}$ follows by reverting the graph of $\mathcal{L}_\beta$ (see Fig. 4). Finally, if we assume that

$$\partial_M \mathcal{L}_\beta(0, \theta) = \frac{3H_*(\theta)}{M_s} - \beta = \frac{3\ell\theta}{M_s} - \beta$$

vanishes at the Curie temperature $\theta = \theta_c$, then we recover the expression (22), namely

$$\beta = 3\ell\theta_c/M_s = \theta_c/C.$$

When $\theta > \theta_c$ ($0 < \beta < 1/\chi_0$), $\mathcal{L}_\beta$ is monotone increasing w.r.t. M, and $f_{L,\beta}$ can be defined by inverting $\mathcal{L}_\beta$. In this case, the Curie–Weiss law holds in the limit of high temperatures, $\theta \gg \theta_c$.

3.3. Phase transition diagram in the (θ, H)-plane

In this subsection, we give a picture of the ferromagnetic transition by relating the temperature and the magnetic field H at which the transition occurs. As a byproduct, we are able to compare this phenomenon to other models of second order transition.

If we restrict our attention to the bilinear model, the change of phase occurs when $\theta < \theta_c$ at $H = H^*_\beta(\theta)$, and then $|H^*_\beta(\theta)|$ can be identified with the *coercive internal field* (see Fig. 3c). By virtue of (14) and (22), we have

$$H^*_\beta(\theta) = M_s/\chi_\beta(\theta) = M_s(\theta - \theta_c)/C.$$

Accordingly, the (θ, H)-plane is divided into four regions, $\mathcal{P}$, $\mathcal{P}^+$, $\mathcal{P}^-$, $\mathcal{M}$, by the lines $H = M_s(\theta - \theta_c)/C$ and $H = -M_s(\theta - \theta_c)/C$, as depicted in Fig. 5. Inside the regions $\mathcal{P}^+$ and $\mathcal{P}^-$ the magnetization keeps the saturation values M_s and $-M_s$, respectively. At a fixed temperature $\theta_1 > \theta_c$, if H takes a value H_1 such that $(\theta_1, H_1) \in \mathcal{P}$, then the magnetization M belongs to $(-M_s, M_s)$. In $\mathcal{P}$, $\mathcal{P}^+$, $\mathcal{P}^-$ the material is in a *unmatched phase* since the values of θ and H determine uniquely the value of M (see Fig. 5a). Otherwise, if $(\theta, H) \in \mathcal{M}$, the gray region, then $M \in (-M_s, M_s)$ because of hysteresis. The material is in a *matched phase*, in that the value of M cannot be uniquely determined by the values of H and θ (see Fig. 5b). Here, H_c stands for the *coercive internal field*.

When the Langevin function is involved, the magnetization M approaches but never reaches the saturation values. If this is the case, Fig. 6 depicts the transition into the (θ, H)-plane and the gray region represents the *matched phases*, where the value of M cannot be uniquely determined by H and θ. This picture is very close to Fig. 7 which represents the (θ, H)-diagram of a second order transition without hysteretic effects, as well as in superconductivity (see, for instance, [5]). Here $\mathcal{N}$ and $\mathcal{S}$ stand for normal and superconducting phases, respectively.

4. A Ginzburg–Landau model for ferromagnetic transitions

In the classical Ginzburg–Landau theory for temperature-induced phase transitions, the evolution equation of the phase parameter φ involves the Gibbs free energy ψ_G and reads

$$\dot{\varphi} = -\epsilon\delta_\varphi\psi_G, \quad \delta_\varphi\psi_G = \partial_\varphi\psi_G - \nabla \cdot \partial_{\nabla\varphi}\psi_G, \tag{24}$$

where the superposed dot denotes the material time derivative and $\epsilon > 0$ is a parameter related to the rate of the transition. This equation is often called *kinetic*, in that it states the drift of the system to recover its equilibrium, which is characterized by the variational condition $\delta_\varphi\psi_G = 0$ (see, for instance, [14]). A more general three-dimensional theory for ferromagnetic

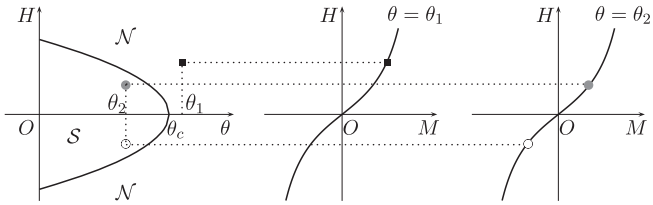

Fig. 7. The (θ, H)-diagram in the superconducting transition and the graphs of f when $\theta = \theta_1 > \theta_c$ (at the center) and $\theta = \theta_2 < \theta_c$ (on the right).

materials was proposed in [12] on the basis of continuum thermodynamics, and a specific evolution equation, which includes the Gilbert–Landau–Lifschitz equation as a special case, is deduced therein.

In a one-dimensional model the phase parameter φ is quite naturally identified with the relative magnetization along the given direction,

$$m = M/M_s, \quad |m| \leqslant 1. \tag{25}$$

Nevertheless, it is worth noting that the phase variable is not necessarily identified with an observable physical quantity, as usual in the Ginzburg–Landau theory of stress-induced transitions in shape-memory alloys [21]. Therefore, a more general relation can be considered here, for instance

$$M = M_s \Gamma(m), \tag{26}$$

where Γ is a monotone non-decreasing function on $(-1, 1)$ which reflects the phenomenological relation between the domain-orientation fraction, m, and the total magnetization, M. From the symmetry of the hysteresis loops, it is expected to be odd, $\Gamma(-m) = -\Gamma(m)$.

Assuming the linear relation (25), we can establish a link to previous approaches. For instance, according to [12, Section 8], the total free energy density is then assumed in the form

$$\psi(H, M, \nabla M, \theta) = \frac{1}{2}\mu_0 H^2 + \Psi(M, \nabla M, \theta) \tag{27}$$

and from [12, Eqn. (6.15)] the evolution of m is ruled by

$$\dot{m} = -\epsilon\left[\theta\delta_m\hat{\psi} - \mu_0\mathcal{H}\right], \quad \hat{\psi} = \psi/\theta, \quad \mathcal{H} = M_s H,$$

where δ_m has the same meaning as δ_φ and $\hat{\psi}$ is referred to as the *rescaled free energy density*. After introducing the Gibbs free energy

$$\psi_G = \psi - HB = \Psi - \frac{1}{2}\mu_0 H^2 - \mu_0 HM, \tag{28}$$

the evolution equation for m takes the form (24) provided that ϵ and ψ_G are replaced by $\epsilon\theta$ and ψ_G/θ, respectively. Taking into account that $\delta_m\psi = \delta_m\Psi = M_s(\partial_M\Psi - \nabla\cdot\partial_{\nabla M}\Psi)$ and splitting Ψ as usual,

$$\Psi(M, \nabla M, \theta) = V(M, \theta) + \frac{1}{2}\kappa|\nabla M|^2,$$

the evolution equation for m transforms into the form [12, Section 8]

$$\dot{m} = -\epsilon M_s\left[\partial_M V - \mu_0 H - \theta\nabla\cdot(\hat{\kappa}\nabla M)\right], \quad \hat{\kappa} = \kappa/\theta.$$

When we restrict our attention to uniform fields ($\nabla M = \boldsymbol{0}$) it reduces to

$$\dot{m} = -\epsilon M_s\left[\partial_M V - \mu_0 H\right] = -\epsilon M_s\partial_M\Phi, \tag{29}$$

where the function $\Phi = V - \mu_0 HM$ can be identified with the Lagrangian density of the system [22]. By means of (25), this phase evolution equation can be rewritten as

$$\dot{M} = -\epsilon M_s^2\partial_M\Phi(H, M, \theta). \tag{30}$$

In the more general case (26), by means of (28) and restricting our attention to uniform fields, the evolution Eq. (24) takes the form

$$\dot{m} = -\epsilon\partial_m\left[V(M_s\Gamma(m), \theta) - \frac{1}{2}\mu_0 H^2 - \mu_0 HM_s\Gamma(m)\right] = -\epsilon M_s\Gamma'(m)[\partial_M V(M_s\Gamma(m), \theta) - \mu_0 H]$$

and then

$$\dot{M} = -\epsilon(M_s\Gamma')^2\partial_M\Phi(H, M, \theta). \tag{31}$$

For definiteness, we choose Γ as either a trigonometric or a polynomial function,

$$\Gamma_1(m) = \sin\frac{\pi m}{2} \quad \text{if } m \in [-1, 1], \quad \Gamma_2 = \frac{1}{2}m(3 - m^2) \quad \text{if } m \in [-1, 1].$$

Although their graphs are very close, it is more convenient to apply the former choice. Indeed, it leads to the useful relation $(\Gamma_1')^2 = \pi^2(1 - \Gamma_1^2)/4$, by means of which Eq. (31) takes the closed form

$$\dot{M} = -\frac{\pi^2\epsilon}{4}(M_s^2 - M^2)\partial_M\Phi(H, M, \theta). \tag{32}$$

Given a suitable initial condition for M, its solution is expected to *recover* the relation (18) in the paramagnetic regime, when $\theta > \theta_c$ and V is convex, and to *replace* it in the ferromagnetic regime, when $\theta < \theta_c$, V is no longer convex and hysteresis occurs.

In order to model the evolution of the ferromagnetic body, Eq. (32) has to be coupled with Maxwell's Eqs. (2) and (3). In addition, possibly, we could append some heat equation in order to rule the evolution of the temperature. The resulting system of differential equations jointly with suitable initial and boundary conditions yields the so-called *thermo-electromagnetic IBVP* (see, for instance, [11]).

4.1. Magnetic potentials from the skeleton curve

A first attempt to give an explicit form to the *magnetic potential* V in (29) traces back to Ginzburg [9]. He proposed the polynomial expression

$$V(M, \theta) = M^2[a(\theta - \theta_c) + bi^2], \quad a, b > 0,$$

which turns out to be non-convex with respect to M when $\theta < \theta_c$. This choice of V leads to gratifying well-posedness results of the thermo-electromagnetic IBVP [11]. Unfortunately, the domain of V spans the whole real axis and the evolution of the magnetization field cannot be confined into $(-M_s, M_s)$. On the contrary, the constraint $|M| < M_s$ is fulfilled *a priori* by the logarithmic potential proposed in [12],

$$V(M, \theta) = -c\left[\frac{\theta}{\theta_c}\ln\left(1 - \frac{M^2}{M_s^2}\right) + \frac{M^2}{M_s^2}\right], \quad c > 0,$$

but no result is available for the corresponding thermo-electromagnetic IBVP.

In the framework of our approach, we prefer to derive rather than assume the expression of the magnetic potential V. In the general case, we start from the thermodynamic relation $d\psi = HdB$, which leads to

$$d\psi = \mu_0(HdH + HdM) = d\left(\frac{1}{2}\mu_0H^2\right) + \mu_0HdM$$

and then from (27) it follows $d\Psi = \mu_0HdM$. When all fields are uniform, we have $d\Psi = dV$, so that

$$dV = \mu_0HdM. \tag{33}$$

This formula can be used to compute V provided that some relation between H and M is given. For instance, we can exploit the shape of the skeleton-curve.

It is worth noting that, accounting for the skeleton-curve representation, in general H can be expressed as a function of M in both paramagnetic and ferromagnetic regimes (see, for instance, Fig. 6). In the former case, namely when $\theta > \theta_c$, from (17) we have $H = g_\beta(M, \theta)$, which is a monotone increasing function w.r.t. M, and this yields the convexity of V. Indeed, from (33) we have

$$\partial_M V(M, \theta) = \mu_0 g_\beta(M, \theta).$$

In the latter case, $\theta < \theta_c$ and g_β is no longer monotone, so leading to a non-convex potential which has the customary shape of a double well. For instance, this procedure can be applied in the Langevin case by noting that $g_{L,\beta} = \mathcal{L}_\beta$, which is given by (23). Then,

$$V_L(M, \theta) = \mu_0\int_0^M \mathcal{L}_\beta(\zeta, \theta)d\zeta = \mu_0H_*(\theta)\int_0^M \mathbb{L}^{-1}(\zeta/M_s) - \mu_0\beta\frac{M^2}{2}, \tag{34}$$

where $M \in (-M_s, M_s)$. This potential is represented by a dotted curve in Fig. 8b when $\theta > \theta_c$ and in Fig. 8d when $\theta < \theta_c$.

The same holds true even in the bilinear case provided that we consider $g_{b,\beta}$ as a maximal monotone graph (see, for instance, Fig. 5a and b). In particular, since $H^* = M_s/\chi_0$, from (20) we obtain

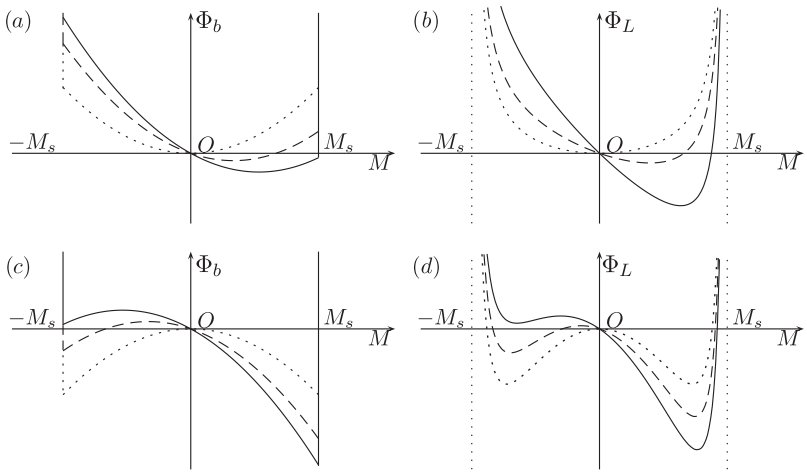

Fig. 8. The graphs of $\Phi_b(H,\cdot,\theta)$ and $\Phi_L(H,\cdot,\theta)$ when $H = 2H^*$ (solid), $H = H^*/2$ (dashed), $H = 0$ (dotted): (a) and (b) at $\theta > \theta_c$; (c) and (d) at $0 < \theta < \theta_c$.

$$g_{b,\beta}(M,\theta) \in \begin{cases} \left\{M/\chi_\beta(\theta)\right\} & \text{if } -M_s < M < M_s, \\ \left[M_s/\chi_\beta(\theta), +\infty\right) & \text{if } M = M_s, \\ \left(-\infty, -M_s/\chi_\beta(\theta)\right] & \text{if } M = -M_s, \end{cases} \tag{35}$$

which is the subdifferential of

$$V_b(M,\theta) = \mu_0 I_{(-M_s,M_s)}(M) + \frac{\mu_0}{2\chi_\beta(\theta)} M^2, \tag{36}$$

where $I_{(a,b)}$ stands for the indicator function of the interval (a,b). This potential is represented by a dotted curve in Fig. 8a when $\theta > \theta_c$ and in Fig. 8c when $\theta < \theta_c$.

4.2. Stability of magnetic equilibria

Now, in order to state the Ginzburg–Landau theory for the paramagnetic–ferromagnetic transition, we only need the complete expression of Φ which enters the evolution Eq. (29), namely

$$\Phi(H,M,\theta) = V(M,\theta) - \mu_0 HM. \tag{37}$$

It refers to a general state (H,M) of the ferromagnetic material at a point x, so that H is independent of M. Then Φ, unlike V, is defined on the whole strip $\mathcal{S} = \mathbb{R} \times [-M_s, M_s]$ of the (H,M)-plane. A different approach is devised in [10], where Φ is identified with the minimum Gibbs free energy and the expression of Φ_b is explicitly obtained by computing the maximum recoverable work. By virtue of (36), it turns out to have exactly the same expression as $V_b(M,\theta) - \mu_0 HM$.

Since in the ferromagnetic phase H and M are independent, the shape of Φ_b and Φ_L can be easily depicted by taking their sections at given values of H. Taking in mind that $V = \Phi|_{H=0}$, we infer that V_b and V_L are represented by the dotted lines of the graphs of Φ_b and Φ_L at $H = 0$, respectively when $\theta > \theta_c$ and $0 < \theta < \theta_c$ (see Fig. 8).

Magnetic potential allow us to scrutinize the equilibria of the system and in particular to identify their stability properties. At a given temperature θ and for any given value of H, the state (H,M) is called *stable* if M is a global minimizer of $\Phi(H,\cdot,\theta)$ on $(-M_s, M_s)$. Depending on the form of the potential at a given temperature, (30) generates the magnetic response as a quasi-static process by connecting stable states. At $\theta > \theta_c$ the potential has a unique minimizer for any value of H (Fig. 8a and b) and the graph of the solution is a single valued curve in the (H,M)-plane. When $\theta < \theta_c$, two absolute minima occurs (Fig. 8c and d): the related Ginzburg–Landau dynamics drives the magnetization M to "jump" from one minimum to the other, so generating the major hysteresis loop. This will be clearly shown in the sequel.

4.3. Numerical simulation in the Langevin case

By means of (30), (34) and (37), in the Langevin case we obtain the evolution equation

$$\dot{M} = -\epsilon\mu_0[\mathcal{L}_\beta(M,\theta) - H].$$

Assuming that H is a time periodic function, for instance $H(t) = A\sin\omega t$, by virtue of (23) we obtain the following evolution system,

$$\begin{cases} \dot{M} = -\epsilon\mu_0\left[H_*(\theta)\mathbb{L}^{-1}(M/M_s) - (H + \beta M)\right] \\ \dot{H} = A\omega\cos\omega t. \end{cases} \tag{38}$$

In Fig. 9 we present the graphs of solutions to this system. All of them start from the origin and are obtained by assuming $A = 2.8,\ M_s = 2,\ \omega = \pi/50$ and $\pi^2\epsilon\mu_0 = 1.2$. The numerical solver is based on a fifth-order Romberg's method. The first graph describes the magnetization curve when $H_*(\theta_1) = 3$. The second and the third graphs represent the initial magnetization curves and the major hysteresis loops when $H_*(\theta_2) = -3$ and $H_*(\theta_3) = -1$, respectively. Of course, $\theta_1 > \theta_c > \theta_2 > \theta_3$. These pictures fit very well the theoretical curves of the Langevin model (cfr. Fig. 4).

4.4. Smoothing and numerical simulation in the bilinear case

At a first sight, the Ginzburg–Landau machinery appears to be unsuitable for modeling the hysteresis loops in the bilinear case, but it is not so. Indeed, the assumption of a suitable nonlinear relation between M and m yields a smoothing in the shape of V and Φ even in the bilinear case.

By applying (26) to replace M into (36) we achieve

$$\Phi_{b,\Gamma}(m,\theta) = \mu_0 I_{(-1,1)}(m) + \frac{\mu_0}{2\chi_\beta(\theta)}M_s^2\Gamma^2(m) - \mu_0 M_s H\Gamma(m).$$

It is easy to check that the resulting graphs of $\Phi_{b,\Gamma}$ with respect to m (see Fig. 10) are smoother than the corresponding graphs of Φ_b (Fig. 8a and c).

What is more, if we replace $\Phi_{b,\Gamma}$ with the following potential which is regular on the whole real line

$$\Phi_{bs,\Gamma} = \frac{\mu_0}{2\chi_\beta(\theta)}M_s^2\Gamma^2(m) - \mu_0 M_s H\Gamma(m), \tag{39}$$

then the end points, $m = 1$ and $m = -1$, provide local maxima or minima and this yields relevant advantages. First of all, this smoothing extension removes the indicator function and then the penalty condition that bounds m in $[-1, 1]$. If this is the case, when finding a solution to thermo-electromagnetic IBVP, we only need to prove *a posteriori* this constraint by virtue of some "maximum theorem" (this was the strategy successfully applied in [11]). In addition, by exploiting this minimum–maximum property of $\Phi_{bs,\Gamma}$, a smart simulation of (32) can be performed.

Assuming that H is a given periodic function of time, for instance $H(t) = A\sin\omega t$, from (32) and (39) (with $\Gamma = \Gamma_1$), we obtain the following evolution system,

$$\begin{cases} \dot{M} = -\frac{\pi^2\epsilon\mu_0}{4}(M_s^2 - M^2)\left(\frac{M}{\chi_\beta} - H\right) \\ \dot{H} = A\omega\cos\omega t. \end{cases} \tag{40}$$

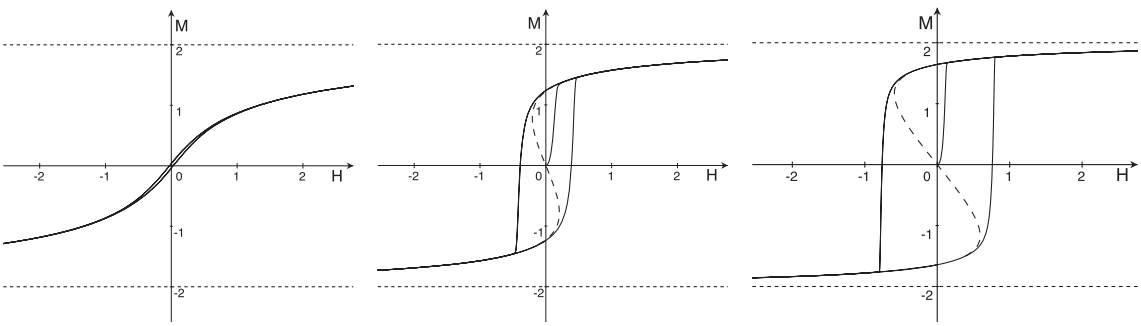

Fig. 9. Numerical simulation of the magnetic responses at different temperatures, $\theta_1 > \theta_2 > \theta_3$, under a cyclic process in H.

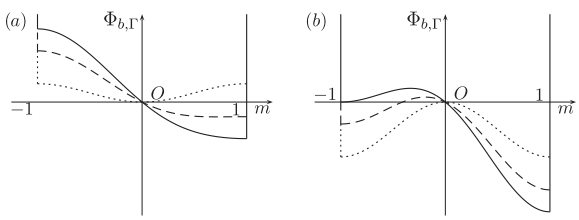

Fig. 10. The graphs of $\Phi_{b,\Gamma}$ when $H = 2H^*$ (solid), $H = H^*/2$ (dashed), $H = 0$ (dotted): (a) at $\theta > \theta_c$; (b) at $0 < \theta < \theta_c$.

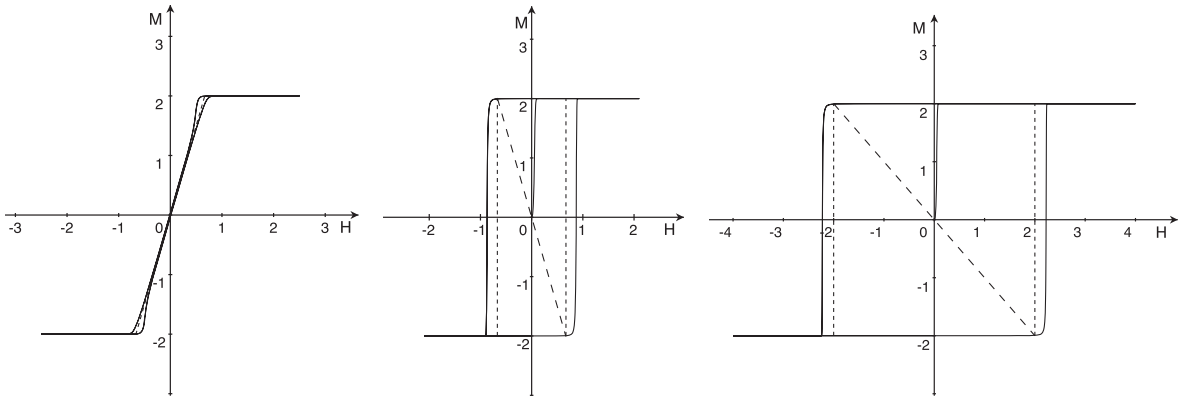

Fig. 11. Magnetic responses at different temperatures, $\theta_1 > \theta_2 > \theta_3$, under a cyclic process in H: numerical simulations (solid), theoretical curves (short dashed), skeleton curves (dashed).

It is worth noting that χ_β depends on θ according to (21). By Remark 3, it follows

$$\chi_\beta(\theta) = \frac{C}{\theta - \theta_c}, \quad C = \frac{M_s^2}{3Nk_B}$$

and then χ_β is negative when $\theta < \theta_c$. In spite of the simplicity and regularity of the resulting model, we show that it is able to capture the main features of the temperature-induced transition.

In Fig. 11 some graphs of solutions to (40) in the (H, M)-plane are presented. All of them start from the origin and are obtained by assuming $M_s = 2$, $\omega = \pi/50$ and $\pi^2\epsilon\mu_0 = 1.2$. The first graph describes the magnetization curve when $A = 2.5$ and $\chi_\beta(\theta_1) = 3$. The second and the third graphs represent the initial magnetization curves and the major hysteresis loops when $A = 2$, $\chi_\beta(\theta_2) = -3$ and $A = 4$, $\chi_\beta(\theta_3) = -1$, respectively. Of course, $\theta_1 > \theta_c > \theta_2 > \theta_3$. These simulations fit very well the theoretical curves of the bilinear model (cfr. Fig. 3).

5. The hysteresis loops in the (H_{ex}, M)-plane

Exploiting the results of the previous sections, the transition between paramagnetic and ferromagnetic regimes is characterized by the occurrence of the hysteresis phenomenon and in particular by the onset of a major loop. This procedure gives rise to "squared" hysteresis loops, as in Figs. 3c and 4c, which do not fit well the so called *soft* ferromagnetic materials. The real shape of the loops emerges in the (H_{ex}, M)-plane description, where $H_{ex} = H + \alpha M$. By means of (6) and (18), the skeleton curves in the (H_{ex}, M)-plane are derived. In general, their shape depends on the sign of the parameter

$$\gamma = \alpha - \beta. \tag{41}$$

Since α and β are positive constants, γ is independent of θ. When $\alpha \geqslant \beta$, then $\gamma \geqslant 0$ and the skeleton curve is monotone increasing w.r.t. H_{ex} for whatever value of the temperature θ. Otherwise, if $\alpha < \beta$, then $\gamma < 0$ and the skeleton curve is monotone increasing only if $\theta > \theta_c$.

5.1. The bilinear case

First, by substituting (6) into relation (20), we obtain the following expression, which represents the *bilinear skeleton curve* in the (H_{ex}, M)-plane:

$$\tilde{f}_{b,\gamma}(H_{ex}, \theta) = \begin{cases} \chi_\gamma(\theta) H_{ex} & \text{if } |H_{ex}| < |1 + \gamma\chi_0| H^*, \\ M_s & \text{if } H_{ex} \geqslant [1 + \gamma\chi_0] H^*, \\ -M_s & \text{if } H_{ex} \leqslant -[1 + \gamma\chi_0] H^*, \end{cases} \tag{42}$$

where $[1 + \gamma\chi_0]H^* = 3\ell\theta + \gamma M_s$, since $\chi_0(\theta) = M_s/3\ell\theta$ and $H^*(\theta) = 3\ell\theta$, and

$$\chi_\gamma(\theta) = \frac{\chi_\beta(\theta)}{1 + \alpha\chi_\beta(\theta)} = \frac{\chi_0(\theta)}{1 + \gamma\chi_0(\theta)}.$$

We stress that χ_γ represents the external susceptibility of the material only when $\theta \geqslant \theta_c$. On the other hand, when the temperature takes values just below the Curie temperature θ_c, hysteresis loops appear after applying, removing and then reversing a large external magnetic field. The loops are characterized by two slopes, 0 and $1/\alpha$, where the latter is the slope which corresponds to the process of the phase change in the (H_{ex}, M)-plane (see the small circles in Figs. 12 and 13). The dependence of the loop shape on α is described in the following remark.

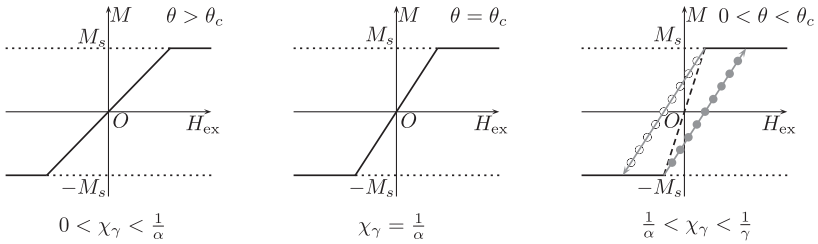

Fig. 12. Soft ferromagnetic materials: $\gamma \geqslant 0$. The graphs of $\tilde{f}_{b,\gamma}$ in the (H_{ex}, M)-plane.

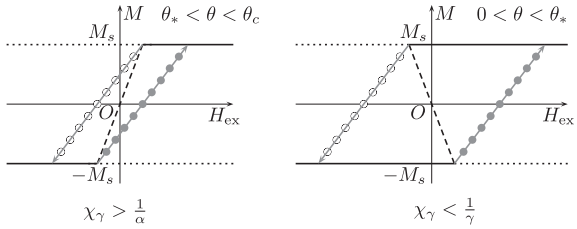

Fig. 13. Hard ferromagnetic materials: $\gamma < 0$. The graphs of $\tilde{f}_{b,\gamma}$ in the (H_{ex}, M)-plane.

Remark 4. The transition occurs when $\theta = \theta_c$ and we have $\chi_0(\theta_c) = 1/\beta,\ \chi_\gamma(\theta_c) = 1/\alpha$. Recalling (14) and (22), when $\theta > \theta_c$ the skeleton slope χ_γ equals the ferromagnetic susceptibility. Its dependence on θ is given by

$$\chi_\gamma(\theta) = \frac{C}{\theta + \gamma C} = \frac{C}{\theta - \theta_c + \alpha C}, \quad C = \frac{M_s}{3\ell}$$

and the Curie–Weiss law still holds in the limit of high temperatures, $\theta \gg \theta_c$. On the other hand, two cases may occur when $0 < \theta < \theta_c$:

- if $\gamma \geqslant 0$ (soft ferromagnetic materials), the skeleton slope differs from the susceptibility and fulfills $1/\alpha < \chi_\gamma(\theta) < 1/\gamma$ (see Fig. 12);
- if $\gamma < 0$ (hard ferromagnetic materials), letting $\theta_* = C|\gamma|$ the skeleton slope still differs from the susceptibility, but fulfills either $\chi_\gamma(\theta) > 1/\alpha > 0$, when $\theta_* < \theta < \theta_c$, or $\chi_\gamma(\theta) < 1/\gamma < 0$, when $0 < \theta < \theta_*$ (see Fig. 13).

A numerical simulation in the (H_{ex}, M)-plane can be easily performed by mimicking the procedure of subSection 4.4. Assuming once again that H is a given periodic function of time, $H(t) = A \sin \omega t$, we recast (40) into the following form

$$\begin{cases} \dot{M} = -\dfrac{\pi^2 \epsilon \mu_0}{4} \left(M_s^2 - M^2\right) \left(\dfrac{M}{\chi_\gamma} - H_{ex}\right) \\ \dot{H}_{ex} = A\omega \cos \omega t - \dfrac{\pi^2 \epsilon \mu_0 \alpha}{4} \left(M_s^2 - M^2\right) \left(\dfrac{M}{\chi_\gamma} - H_{ex}\right) \end{cases} \tag{43}$$

Here, χ_γ depends on θ according to Remark 4.

Hereafter, we show the resulting simulation for both soft and hard ferromagnetic samples, respectively. All solutions to (43) start from the origin and are obtained by assuming $M_s = 2,\ \omega = \pi/50,\ \pi^2 \epsilon \mu_0 = 1.2,\ A = 1.8$ and $\alpha = 2/3$. For a soft

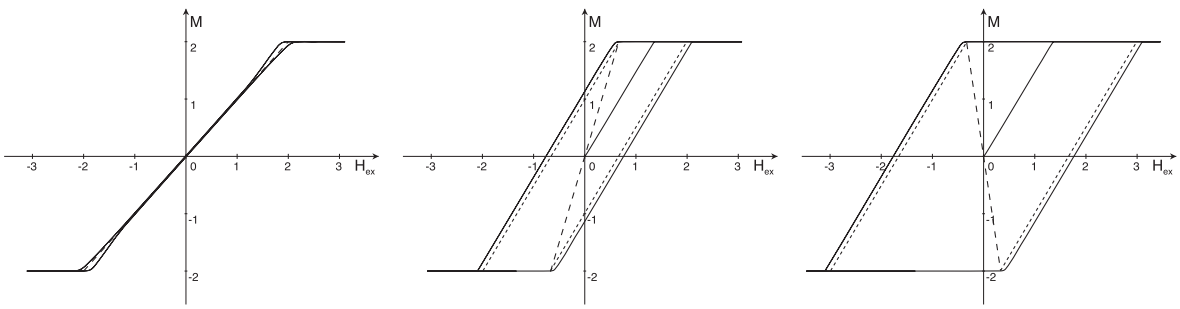

Fig. 14. Soft and hard ferromagnetic responses at different temperatures: numerical (solid), theoretic (short dashed), skeleton (dashed).

material ($\gamma = 1/4$), Fig. 14 describes the magnetization curve in the paramagnetic regime when $\chi_\gamma(\theta_1) = 1$ (on the left) and the major hysteresis loop when $\chi_\gamma(\theta_2) = 3$ (at the center), and $\theta_1 > \theta_c > \theta_2$.

On the other hand, for a hard material ($\gamma = -1/4$), Fig. 14 describes the magnetization curve in the paramagnetic regime when $\chi_\gamma(\theta_1) = 1$ (on the left) and the major hysteresis loops when $\chi_\gamma(\theta_2) = 3$ (at the center) and $\chi_\gamma(\theta_3) = -6$ (on the right). Of course, $\theta_1 > \theta_c > \theta_2 > \theta_* > \theta_3$.

5.2. The Langevin case

Finally, by substituting (6) into relation (23), we obtain

$$H_{\text{ex}} = \mathcal{L}_\gamma(M, \theta) \equiv H_*(\theta)\mathbb{L}^{-1}(M/M_s) + \gamma M.$$

By inverting this function (piece-wisely, possibly) we construct $\tilde{f}_{L,\gamma}$, which represents the *Langevin skeleton curve* in the (H_{ex}, M)-plane. In particular,

$$\partial_M \mathcal{L}_\gamma(0, \theta) = \frac{3\ell\theta}{M_s} + \gamma$$

and the slope of the skeleton curve $\tilde{f}_{L,\gamma}$ in $H_{\text{ex}} = 0$ is

$$\partial_{H_{\text{ex}}} \tilde{f}_{L,\gamma}(0, \theta) = \frac{C}{\theta - \theta_c + \alpha C},$$

as well as in the bilinear case. Then, at $\theta = \theta_c$ the slope of the skeleton curve $\tilde{f}_{L,\gamma}$ in $H_{\text{ex}} = 0$ is $1/\alpha$.

A numerical simulation in the (H_{ex}, M)-plane can be easily performed by mimicking the procedure of subSection 4.3. Assuming once again $H(t) = A \sin \omega t$, we recast (38) into the following form

$$\begin{cases} \dot{M} = -\epsilon\mu_0 \left[H_*(\theta)\mathbb{L}^{-1}(M/M_s) + \gamma M - H_{\text{ex}}\right] \\ \dot{H}_{\text{ex}} = A\omega \cos \omega t - \epsilon\mu_0 \alpha \left[H_*(\theta)\mathbb{L}^{-1}(M/M_s) + \gamma M - H_{\text{ex}}\right]. \end{cases} \tag{44}$$

All solutions to (44) in Fig. 15 start from the origin and are obtained by assuming $M_s = 2$, $\omega = \pi/50$, $\pi^2\epsilon\mu_0 = 1.2$, $A = 1.8$, $\alpha = 2/3$ and $\gamma = -1/4$. They describe the magnetization curves when the slope of the skeleton curve in $H_{\text{ex}} = 0$ is equal to $1 < 1/\alpha$ (paramagnetic regime) and when it is equal to $10 > 1/\alpha$ and equal to -6 (ferromagnetic regime), respectively at temperatures $\theta_1(> \theta_c) > \theta_2(> \theta_*) > \theta_3$.

6. Dependence of the ferromagnetic susceptibility on the temperature

In this section we restrict our attention to the bilinear model for soft ferromagnetic materials, hence we assume $\gamma > 0$, namely $\alpha > \beta$. Our aim is to determine the general form of the external ferromagnetic susceptibility, $\chi_{\text{ex}}^{\text{fm}}$, that is the slope of the phase-change process in the (H_{ex}, M)-plane.

In the previous section, α was assumed to be independent of the temperature, as well as β. Accordingly, we established that $\chi_{\text{ex}}^{\text{fm}}$ is constant and equal to $1/\alpha$ for every $\theta \in (0, \theta_c]$. Really, the constancy of α in $(0, \theta_c]$ was implicitly introduced in Remark 1 just in order to simplify the description of the model, but it can be easily removed.

Thereafter, we scrutinize a more general case, where $\chi_{\text{ex}}^{\text{fm}}$ is an unknown function which may depend on the temperature in $(0, \theta_c]$. By exploiting the Bloch's law, we obtain the general shape of this function. Then we ask for the choice of α on $(0, \theta_c]$ which allows the Ginzburg–Landau model to be consistent with it.

In the paramagnetic regime, $\chi_{\text{ex}}^{\text{fm}}$ equals the slope of the skeleton curve,

$$\chi_{\text{ex}}^{\text{fm}}(\theta, \theta_c) = \chi_\gamma(\theta), \quad \theta > \theta_c,$$

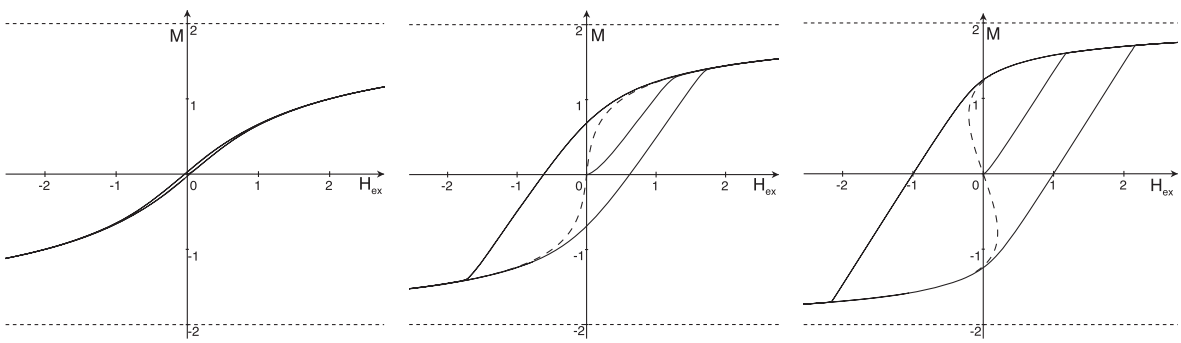

Fig. 15. Hard ferromagnetic responses at different temperatures (at $\theta_1 > \theta_c$ on the left, at $\theta_* < \theta_2 < \theta_c$ in the center, at $\theta_3 < \theta_*$ on the right) under a cyclic process in H_{ex}: numerical simulations (solid) and skeleton curves (dashed).

whose dependence on the temperature has been previously discussed and proved to match the Curie–Weiss law for large values of θ. In the ferromagnetic regime, χ_{ex}^{fm} is a positive function of the temperature which matches the value of χ_γ at $\theta = \theta_c$, namely

$$\chi_{ex}^{fm}(\theta_c, \theta_c) = \chi_\gamma(\theta_c) = 1/\alpha.$$

In order to explicitly compute the expression of $\chi_{ex}^{fm}(\theta, \theta_c)$ even when $\theta < \theta_c$, we introduce a constant $\nu \in (0, 1]$ and a continuous function τ such that

$$\chi_{ex}^{fm}(\theta, \theta_c) = \begin{cases} \chi_\gamma(\theta) & \text{if } \theta > \theta_c \\ 1/\alpha & \text{if } \theta = \theta_c \\ \chi_\gamma(\theta)[1 - \nu\tau(\theta)] & \text{if } 0 < \theta < \theta_c, \end{cases}$$

where τ satisfies the following conditions:

$$0 < \tau(\theta) < 1, \quad 0 < \theta < \theta_c, \quad \tau(0) = 1.$$

According to these assumptions, we notice that

$$\chi_{ex}^{fm}(\theta, \theta_c) < \chi_\gamma(\theta), \quad 0 < \theta < \theta_c,$$

which is consistent with the hysteretic phenomena. In addition,

$$\chi_{ex}^{fm}(0, \theta_c) = \chi_\gamma(0)[1 - \nu\tau(0)] = 1 - \nu/\gamma > 0.$$

On the other hand, when θ increases and overcomes the critical value θ_c, then $\chi_{ex}^{fm}(\theta, \theta_c) = \chi_\gamma(\theta)$, hysteresis loops disappear and the major loop reduces to the skeleton curve.

Since we know the expression of χ_γ for any $\theta > 0$, we have to establish the dependence of τ on θ. To this end, we introduce the remnant (or spontaneous) magnetization M_r, which can be evaluated as the intersection of the major hysteresis loop with the vertical magnetization axis, namely

$$M_r(\theta) = M_s\left[1 - \frac{\chi_{ex}^{fm}(\theta, \theta_c)}{\chi_\gamma(\theta)}\right] = M_s\nu\tau(\theta). \tag{45}$$

For a large class of materials, the spontaneous magnetization M_r complies with the generalized Bloch's law (see, for instance, [2, p. 246])

$$M_r(\theta) = M_r^\circ\left[1 - (\theta/\theta_c)^\lambda\right], \quad 0 < \theta < \theta_c, \tag{46}$$

where $M_r^\circ = M_r(0) \leqslant M_s$ and $\lambda > 1$. Hereafter we assume $\lambda = 3/2$, according to quantum mechanics (see [4,2]). Although the dependence of the spontaneous magnetization on temperature differs from Bloch's law in a variety of ferromagnetic and ferrimagnetic garnets (see, for instance, [2, p. 517]), our procedure is able to exactly evaluate the expression for τ even in these cases, by merely inserting the experimental form of $M_r(\theta)$ into (45).

From comparing (45) and (46), evaluated at $\theta = 0$, it follows

$$\nu = M_r^\circ/M_s \tag{47}$$

and then we easily obtain

$$\tau(\theta) = 1 - (\theta/\theta_c)^\lambda.$$

Accordingly, when $0 < \theta < \theta_c$ we have

$$\chi_{ex}^{fm}(\theta, \theta_c) = \chi_\gamma(\theta)\left\{1 - \nu\left[1 - (\theta/\theta_c)^\lambda\right]\right\}.$$

Recalling the dependence of χ_γ on θ, we obtain

$$\chi_{ex}^{fm}(\theta, \theta_c) = \begin{cases} \frac{C}{\theta - \theta_c + \alpha C}\left\{1 - \nu\left[1 - (\theta/\theta_c)^\lambda\right]\right\} & 0 < \theta < \theta_c, \\ \frac{C}{\theta - \theta_c + \alpha C} & \theta \geqslant \theta_c. \end{cases} \tag{48}$$

Its graph is depicted in Fig. 16 (a close result was achieved in [10]).

Finally, we have to justify the assumption made in Section 5,

$$\chi_{ex}^{fm}(\theta, \theta_c) = 1/\alpha \quad \forall\theta \in (0, \theta_c].$$

If α is assumed to be constant, then we need to choose its value in such a way that $(1 - \nu)/\gamma = 1/\alpha$ and then $\alpha = \beta/\nu$. In view of (47), $(14)_2$ and (22), we finally obtain the restrictions

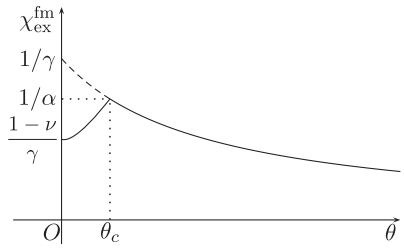

Fig. 16. The graphs of χ_{ex}^{fm} (solid) and χ_γ (dashed) when $\nu = \gamma = 1/2,\ \alpha = \frac{1}{\lambda} = 2/3$.

$$\alpha = \frac{M_s\theta_c}{M_r^\circ C} = \frac{3Nk_B\theta_c}{M_r^\circ M_s}, \quad \gamma = \alpha(1-\nu) = 3Nk_B\theta_c\frac{M_s - M_r^\circ}{M_r^\circ M_s^2},$$

which do not seem to be justified from the physical point of view.

Alternately, we may allow the material factor α to depend on θ. In view of (48), we replace α with the function

$$\hat{\alpha}(\theta,\theta_c) = \frac{\theta - \theta_c + \alpha C}{C\left\{1 - \nu\left[1 - (\theta/\theta_c)^\lambda\right]\right\}} \quad 0 < \theta < \theta_c,$$

where $\alpha = \hat{\alpha}(\theta_c,\theta_c) > \beta$. Finally, it is easy to check that $\hat{\alpha}(\theta,\theta_c) > \beta$ for all $\theta \in (0,\theta_c]$, since $\hat{\alpha}$ is a decreasing function.

7. Conclusions

The analysis devised here relies on the paper by Fabrizio et al. [12] where the Ginzburg–Landau theory for a ferromagnetic material is derived in a suitable thermodynamic framework. When considered along a fixed alignment (see [12] subSection 6.1), the vector-valued phase evolution equation reduces to the scalar Ginzburg–Landau-like Eq. (24). The resulting models differ by (and take advantage of) the expression of the Gibbs free energy (28). On this basis, we develop and discuss here two new basic one-dimensional models of the *ferromagnetic behavior*, which account for magnetic saturation. The former is called *bilinear* from the shape of the skeleton curve which is used to compute its potential (39). The latter is developed from a physics-based shape of the skeleton curve, which is referred to as *Langevin* function, and then it is accordingly named: this choice leads to the energy potential (34).

The main features to emerge from this paper are summarized as follows. Due to its thermodynamic framework, the phase evolution equation is naturally energy consistent. The phase variable is related to the magnetization, but does not coincide with it: this enable us to manage the bilinear case by means of a regular potential (subSection 4.4). The temperature-induced transition from paramagnetic to ferromagnetic regimes is characterized by the onset of a major loop, that is a region where stable states are not uniquely determined by H (see Figs. 3 and 4). By properly introducing the notion of *matched* and *unmatched* phases (see Definition 1), transitions turn out to be driven by varying either the temperature or the magnetic field, as expected. As a consequence, the ferromagnetic (θ, H)-diagram can be compared with the corresponding diagram in superconductivity (see Figs. 6 and 7). Both bilinear and Langevin models properly describe soft and hard ferromagnetic materials: the former leads to "box-shaped" hysteresis loops, whereas the latter reproduces more regular loops (see Figs. 11 and 9). This approach reveals to be effective by comparing theoretical results to numerical simulations when cyclic processes are involved, and this clearly emerges from the (H_{ex}, M)-plane description, where H_{ex} is the external applied field (see Figs. 14 and 15). Finally, by exploiting the Bloch's law, in (48) we establish the general shape of the external ferromagnetic susceptibility, $\chi_{ex}^{fm}(\theta,\theta_c)$, which is consistent with the bilinear model for soft ferromagnetic materials.

Extending the analysis to more convincing models might be the object of future projects. In particular, further research might be devoted to extend the Langevin model devised here to the three dimensional case, so including the rotating property of the magnetization [12], and then compare the resulting evolution system with the recently proposed VINCH model [23].

References

[1] J.M.D. Coey, Magnetism and Magnetic Materials, Cambridge University Press, Cambridge, 2009.
[2] A.H. Morrish, The Physical Principles of Magnetism, Wiley-IEEE Press, New York, 2001.
[3] M. Brokate, J. Sprekels, Hysteresis and Phase Transitions, Springer, New York, 1996.
[4] L.D. Landau, E.M. Lifshitz, L.P. Pitaevskii, Statistical Physics, Pergamon, Oxford, 1980.
[5] L.D. Landau, V.L. Ginzburg, On the theory of superconductivity, in: D. ter Haar (Ed.), Collected Papers of L.D. Landau, Pergamon Press, Oxford, 1965.
[6] G. Bertotti, I.D. Mayergoyz, The Science of Hysteresis: Mathematical Modeling and Applications, vol. 1, Academic Press, Oxford, 2006.
[7] A. Visintin, Differential Models of Hysteresis, Series: Applied Mathematical Sciences, vol. 111, Springer, Berlin, 1994.
[8] V.I. Levitas, D.L. Preston, Three-dimensional Landau theory for multivariant stress-induced martensitic phase transformations. I. Austenite ↔ martensite, Phys. Rev. B 66 (2002) 134–206.
[9] L.D. Landau, E.M. Lifshitz, L.P. Pitaevskii, Electrodynamics of Continuous Media, Pergamon, Oxford, 1984. Section 39.

[10] A. Berti, C. Giorgi, E. Vuk, Free energies in one-dimensional models of magnetic transitions with hysteresis, Nuovo Cimento Soc. Ital. Fis. B 125 (4) (2010) 371–394.
[11] V. Berti, M. Fabrizio, C. Giorgi, A three-dimensional phase transition model in ferromagnetism: existence and uniqueness, J. Math. Anal. Appl. 355 (2) (2009) 661–674.
[12] M. Fabrizio, C. Giorgi, A. Morro, Phase transition in ferromagnetism, Int. J. Eng. Sci. 47 (2009) 821–839.
[13] M. Fabrizio, G. Matarazzo, M. Pecoraro, Hysteresis loops for para-ferromagnetic phase transitions, Z. Angew. Math. Phys. 62 (2011) 1013–1026.
[14] M. Fabrizio, C. Giorgi, A. Morro, A thermodynamic approach to non-isothermal phase-field evolution in continuum physics, Phys. D 214 (2006) 144–156.
[15] A. Berti, C. Giorgi, E. Vuk, First-order phase transitions and hysteresis, to appear in Acta Applicandae Mathematicae.
[16] V. Berti, M. Fabrizio, D. Grandi, Phase transitions in shape memory alloys: a non-isothermal Ginzburg–Landau model, Phys. D 239 (2010) 95–102.
[17] M. Fabrizio, A. Morro, Electromagnetism of Continuous Media, Oxford University Press, Oxford, 2003.
[18] W.F. Brown Jr., Micromagnetics, Interscience Tracts on Physics and Astronomy, 18, Interscience Publishers, New York, 1963.
[19] B.D. Cullity, C.D. Graham, Introduction to Magnetic Materials, second ed., Wiley-IEEE Press, New York, 2008.
[20] D.L. Atherton, D.C. Jiles, Theory of ferromagnetic hysteresis, J. Magn. Magn. Mater. 61 (1986) 48–60.
[21] A. Berti, C. Giorgi, E. Vuk, Free energies and pseudo-elastic transitions for shape memory alloys, Discrete Cont. Dyn. Syst. Ser. S 6 (2013) 293–316.
[22] N. Goldenfeld, Lectures on Phase Transitions and the Renormalization Group, Addison-Wesley, New York, 1992. p. 177.
[23] V. François-Lavet, F. Henrotte, L. Stainier, L. Noels, C. Geuzaine, An energy-based variational model of ferromagnetic hysteresis for finite element computations, J. Comput. Appl. Math. 246 (2013) 243–250.